Colloid Polym Sci
DOI 10.1007/s00396-013-3071-1

ORIGINAL CONTRIBUTION

Colloidal stability evolution and completely reversible aggregation of gold nanoparticles functionalized with rationally designed free radical initiators

Hye Hun Park · Hansoo Park · Andrew C. Jamison · T. Randall Lee

Received: 3 April 2013 / Revised: 6 September 2013 / Accepted: 8 September 2013

Abstract A series of molecular adsorbates having various chain lengths of terminal poly(ethylene glycol methyl ether) (PEG) moieties, thiol head groups, and intervening free radical initiator moieties was used to functionalize the surface of gold nanoparticles (AuNPs). The bulky PEG groups stabilized the functionalized AuNPs by providing steric hindrance against AuNP aggregation, such aggregation being a major problem in the modification and manipulation of metal nanoparticles. UV–vis spectroscopy was used to evaluate the stability of the adsorbate-functionalized AuNPs as a function of AuNP size (~15, 40, and 90 nm in diameter) and PEG chain length (Mn 350, 750, and 2,000). The longer PEG chains (Mn 750 and 2,000) afforded stability to AuNPs with smaller gold cores (~15 and 40 nm in diameter) for up to several days without any marked aggregation. In contrast, the adsorbate-functionalized AuNPs with the largest gold cores (~90 nm) were noticeably less stable than those with the smaller gold cores. Importantly, the adsorbate-functionalized AuNPs could be isolated in solvent-free "dried" form and readily dispersed in aqueous buffer solution (both acidic and basic) and various organic solvents (protic and aprotic). This isolation–redispersion (i.e., aggregation/deaggregation) process was completely reversible. The chemisorption of the PEG-terminated initiator on the surface of the AuNPs was verified by Fourier transform infrared (FT-IR) spectroscopy and X-ray photoelectron spectroscopy (XPS). As a whole, the strategy reported here affords colloidally stable, free radical initiator-functionalized AuNPs and offers a promising general method for encapsulating metal nanoparticles within polymer shells.

Keywords Temperature responsive · pH responsive · Hydrogel nanoparticles · Gold nanoparticles · Gold core-polymer shell · Drug delivery

H. H. Park · A. C. Jamison · T. R. Lee (✉)
Department of Chemistry and Texas Center for Superconductivity, University of Houston, Houston 77204-5003, USA
e-mail: trlee@uh.edu

H. H. Park
Molecular Recognition Research Center, Korea Institute of Science and Technology, P. O. Box 131, Cheongryang, Seoul 130-650, South Korea

H. Park
School of Integrative Engineering, Chung-Ang University, Seoul 156-756, South Korea

Introduction

The fabrication of polymer shell/metal core nanoparticle architectures in which a layer of polymer material surrounds an inorganic core has been the focus of numerous publications owing to potential applications in fields of research ranging from optics [1–3], to electronics [4], to catalysis [5, 6]. Such applications typically involve tailoring the surface properties of the core particles by coating and encapsulating them within a desired polymeric material. Some of the physical and chemical properties of the core nanoparticles are often imparted to the resulting polymeric shell system, producing hybrid materials with novel properties and functions that are not possible from the single-component structure alone. Among the various polymer shell/metal core structures of particular interest is the encapsulation of gold nanoparticles (AuNPs) within functional polymers [7–10]. Such systems are attractive due to their biocompatibility [11–13], ease of functionalization because of the strong thiol–gold bond [14], and optical properties related to the gold core and its surface plasmon characteristics, which arise from light coupling to the collective oscillation of the conduction band electrons of the metal [15].

There are two general methods for producing a polymer shell around a gold nanoparticle: the "grafting to" and the "grafting from" methods. In the "grafting to" method, a

Published online: 11 October 2013

polymer molecule is grafted (covalently bonded) to the surface of the AuNP [16, 17]. In the "grafting from" method, however, the preferred polymer is grown from the surface of the nanoparticles via a process known as "surface-induced" of "surface-initiated" polymerization [7–9]. To generate a polymer shell using the "grafting from" method, a polymerization initiator is immobilized on the surface of the AuNPs, and preferred monomers are polymerized on the surface of the particles using the immobilized initiators. This process typically leads to a high polymer chain density on the surface of the nanoparticle because the relatively small initiator molecules can completely cover the gold surface. Furthermore, the uniformity and thickness of the polymer shell can also be controlled, allowing the fabrication of well-designed composite nanoparticles.

The immobilization of small molecules on the surface of AuNPs, however, often allows for irreversible aggregation of the resulting initiator-modified AuNPs, which is a major drawback to the fabrication of polymer shell/metal core nanocomposite structures. In general, colloidal particles in a dispersion medium are subject to Brownian motion, and this produces frequent collisions between particles [18]. During such a collision, there are two basic interactions between the particles that determine their stability: one being the attractive forces (van der Waals attractive forces often dominated by a metallic core) and the other being the repulsive forces (mainly electrostatic and steric hindrance). If the attractive forces dominate, the particles will aggregate; in contrast, if the repulsive forces dominate, the system will remain in a dispersed, stable state. For nanoparticles in solution, due to the van der Waals attractive forces acting continuously between them, it is necessary to introduce a repulsive force to maintain particle stability [19]. For example, AuNPs are commonly synthesized through the reduction of auric acids in water using trisodium citrate, with the citrate ions also serving as stabilizing ligands providing surface-bound negative charges, repulsive electrostatic forces around the AuNPs [20]. Upon the chemisorption of electrostatically neutral small molecules, the molecules displace citrate ions from the AuNP surface, reducing or eliminating the surface charges [21]. Without strong charge–charge repulsions, these monolayer-coated AuNPs can be driven to each other by van der Waals attractions, leading to aggregation. In most cases, aggregation of AuNPs is an irreversible process, and the presence of irreversibly aggregated AuNPs changes the particle size distribution, optical properties, and the surface-to-volume ratio for the AuNPs in solution, making it difficult or impossible to employ them in various applications [22, 23].

A number of methods have been described for stabilizing AuNPs, including but not limited to the physisorption of polyoxyethylene (20) sorbitan monolaurate (Tween 20) [24], direct attachment of bolaamphiphile surfactants [25] or thiolated polymers [26], and layer-by-layer deposition of polymers using charge interactions on the surface of AuNPs as a driving force [27]. Reversible aggregation/deaggregation of AuNPs, which is an important consideration for the development of reusable AuNPs as well as in the development of a fundamental understanding of the nature of the interactions between the particles, is even more difficult to realize. Surfactant molecules bound to the aggregated NPs have a tendency to collapse or be displaced, allowing the metal cores to fuse together irreversibly, giving rise to larger, insoluble materials [23, 28].

We report here the reversible aggregation/deaggregation of AuNPs functionalized with adsorbates having various chain lengths of terminal poly(ethylene glycol methyl ether) (PEG) moieties, thiol head groups, and intervening free radical initiator moieties (see Fig. 1). For these adsorbates, the thiol group at one end of the chain is utilized to anchor these surfactants to the AuNP surface by Au–S bond formation, and the PEG groups at the other end are used to stabilize the AuNPs via steric hindrance. In a selected example utilizing this architecture, the intervening initiator moieties were shown to promote the growth of poly(*N*-isopropylacrylamide) (PNIPAM) hydrogel coatings on AuNPs [29]. In the present investigation, the stability of the adsorbate-functionalized nanoparticles in water was evaluated as a function of nanoparticle size (~15, 40, and 90 nm in diameter) as well as PEG chain length (Mn 0, 350, 750, and 2,000). The AuNPs stabilized with the PEG750-modified initiator were isolated in solvent-free "dried" form and then redispersed in aqueous buffer solutions (pH 4, 7, and 10) and in nonaqueous solvents such as ethanol (EtOH), methanol (MeOH), tetrahydrofuran (THF), and dichloromethane (CH_2Cl_2), where the aggregation/deaggregation was fully reversible. These reversible systems were monitored with the naked eye and more precisely tracked with UV–vis measurements of absorption/scattering of light by the nanoparticles (i.e., the extinction spectra). As a whole, these studies provide useful cues to the assembly of stable, free radical initiator/gold core nanoparticles capable of being encapsulated with polymer shells, offering ready variability in the nature of both the core particles and the polymer shells.

Experimental section

Materials

For the adsorbate syntheses, 4,4′-azobis(4-cyanovaleric acid) (Aldrich, 75+%), 1,6-hexanedithiol (Aldrich, 96.0 %), PEG (Aldrich; Mn 350, 750, and 2,000), *N*,*N*′-dicyclohexylcarbodiimide (DCC; Fluka, 99.0 %), and 4-dimethylaminopyridine (DMAP; Acros, 99.0 %) were used as received. THF (Mallinckrodt Baker) was freshly distilled over calcium hydride and collected immediately prior to use. Absolute EtOH was purchased from McCormick Distilling

Co. and used as purchased. Hexane, ethyl acetate, chloroform ($CHCl_3$), CH_2Cl_2, and MeOH were purchased from Mallinckrodt Baker and used without further purification. In the preparation of gold nanoparticles, trisodium citrate (EM Sciences, 99.0 %), and hydrogen tetrachloroaurate (Strem, 99.9 %) were used as received. All water used in the reactions was purified to a resistance of 18 MΩ (Milli-Q Reagent Water System, Millipore Corporation) and filtered through a 0.2-μm filter to remove any particulate matter.

Synthesis of the initiator-containing adsorbate molecules

The strategy used to prepare the three PEG-terminated free radical initiators is shown in Fig. 1, where each of the compounds shares a common thiol-terminated intermediate, identified as HS–NN–, but having the formal name (R)-4-cyano-4-((E)-((R)-2-cyano-5-(6-mercaptohexylthio)-5-oxopentan-2-yl)diazenyl)-pentanoic acid. Notably, the syntheses of HS-NN- and (E)-PEG750-4-cyano-4-((E)-((R)-2-cyano-5-(6-mercaptohexylthio)-5-oxopentan-2-yl)diazenyl)pentanoic acid (denoted as HSPEG750) were reported previously [29].

(E)-PEG350-4-cyano-4-((E)-((R)-2-cyano-5-(6-mercaptohexylthio)-5-oxopentan-2-yl)diazenyl)pentanoic acid (HSPEG350) The pendant end of the pure thiolated acid (HS–NN–) was further modified with the PEG350 moiety using a DCC/DMAP method. Under an atmosphere of argon, 1.00 g (2.43 mmol) of the pure thiolated acid and 0.85 g (2.4 mmol) of poly(ethylene glycol) methyl ether (Mn 350, PEG350) and 30 mg (0.25 mmol) of DMAP were dissolved in 50 mL of anhydrous THF. The solution was cooled to 0 °C and 0.60 g (2.9 mmol) of DCC in 30 mL of THF was added dropwise to the mixture with stirring. The reaction mixture was allowed to react at 0 °C for 30 min and then warmed to room temperature and stirred for 24 h under argon. The urea precipitate was removed by filtration, and the filtrate was poured into saturated sodium bicarbonate, extracted with CH_2Cl_2, and dried over magnesium sulfate. After the solvent was evaporated, the product was further purified by chromatography on silica gel using 95:5 CH_2Cl_2/MeOH as eluent to give the desired product as a clear oil (0.57 g, 0.76 mmol). Yield was 30 %. ^{1}H NMR (in $CDCl_3$, δ in ppm): 4.26 (t, J= 3.3 Hz, 2H), 3.73–3.53 (m, 35H), 3.38 (s, 3H), 2.89 (t, J= 6.9 Hz, 2H), 2.49 (m, 10H), 1.73 (s, 3H), 1.68 (s, 3H), 1.58 (p, J=7.2 Hz, 4H), and 1.38 (m, 4H).

(E)-PEG2000-4-cyano-4-((E)-((R)-2-cyano-5-(6-mercaptohexylthio)-5-oxopentan-2-yl)diazenyl)pentanoic acid (HSPEG2000) The pendant end of the pure thiolated acid (HS–NN–) was further modified with the PEG2000 moiety using the DCC/DMAP method used in the synthesis of HSPEG350. After the reaction, the urea precipitate was removed by filtration, and the filtrate was poured into saturated sodium bicarbonate, extracted with CH_2Cl_2, and dried over magnesium sulfate. The solvent was evaporated and the product was further purified by chromatography on silica gel using 90:10 CH_2Cl_2/MeOH as eluent to give the desired product as a white solid (1.21 g, 0.51 mmol). Yield was 20 %. ^{1}H NMR (in $CDCl_3$, δ in ppm): 4.26 (t, J=3.3 Hz, 2H), 3.79–3.49 (m, 196H), 3.38 (s, 3H), 2.89 (t, J=6.9 Hz, 2H), 2.49 (m, 10H), 1.73 (s, 3H), 1.68 (s, 3H), 1.58 (p, J=7.2 Hz, 4H), and 1.38 (m, 4H).

Preparation of AuNPs

Three different sizes of AuNPs (~15, 40, and 90 nm in diameter) were prepared by the conventional citric acid reduction of $HAuCl_4$ in water with trisodium citrate at a near-boiling temperature [30]. The size of the AuNPs was

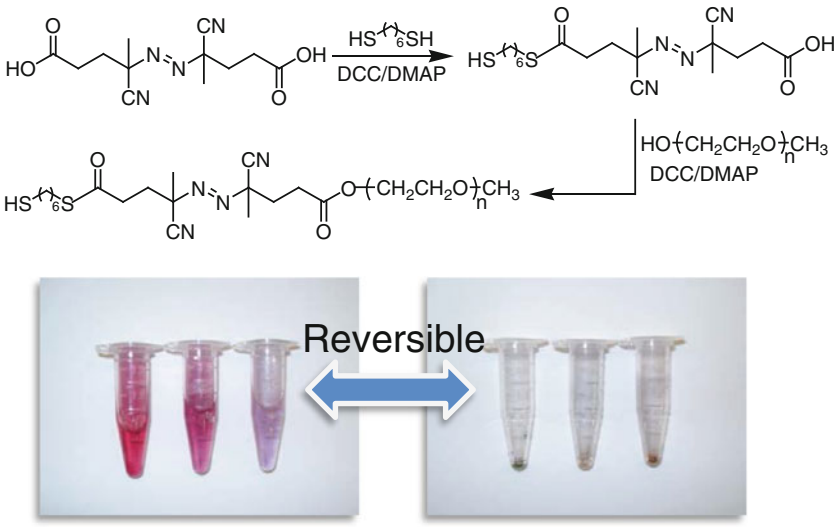

Fig. 1 Strategy used to prepare the initiators (HSPEG350, HSPEG750, and HSPEG2000, where n =~7, 16, and 45, respectively) and a schematic illustrating the reversible aggregation/deaggregation of the HSPEG-functionalized AuNPs

characterized by scanning electron microscopy (SEM) and dynamic light scattering (DLS). All glassware used in the preparation and storage of the AuNPs were treated with aqua regia, rinsed with purified water, and cleaned with piranha solution (7:3 concentrated H_2SO_4/30 wt% H_2O_2). *Caution: piranha solution reacts violently with organic materials and should be handled carefully!*

Immobilization of the initiator-containing adsorbates on the surface of the AuNPs

Ten milliliters of each AuNP solution (15 nm; ~3×10^{11} particles/mL, 40 nm; ~8×10^{10} particles/mL, 90 nm; ~7×10^{9} particles/mL) was mixed with a 1-mM solution of each adsorbate (HSPEG350, HSPEG750, and HSPEG2000) in ethanol (3 mL) for 30 min, and the resulting mixture was allowed to stand at room temperature for 24 h. To remove any unbound adsorbate molecules, the final mixture was washed by centrifugation at 8,000, 6,000, and 3,000 rpm for the ~15, 40, and 90 nm gold core nanoparticles, respectively, for 30 min each. This rinse procedure was conducted twice with water and twice with EtOH.

Characterization of the molecular adsorbates, AuNPs, and adsorbate-functionalized AuNPs

Nuclear magnetic resonance (NMR) spectra were recorded on a General Electric QE-300 spectrometer operating at 300 MHz for ^{1}H NMR. The data for the organic syntheses were collected in $CDCl_3$ and referenced to the residual ^{1}H peak at δ 7.26. To characterize the bare and modified AuNPs and to verify the assembly of adsorbate-functionalized AuNPs, ultraviolet–visible (UV–vis) spectroscopy, Fourier transform infrared (FT-IR) spectroscopy, X-ray photoelectron spectroscopy (XPS), SEM, transmission electron microscopy (TEM), and DLS were used.

The extinction spectra of the AuNPs and the adsorbate-functionalized AuNPs were measured at room temperature using a Cary 50 Scan UV–vis optical spectrometer (Varian) with Cary Win UV software employed. Extinction spectra of the prepared AuNPs in aqueous solution were collected in a quartz cuvette having a 1-cm optical path length, scanning over a range of wavelengths (400–1,000 nm). The measurements for the solvent-free form (prepared by depositing one drop of each of the HSPEG750-AuNPs (~15, 40, and 90 nm gold cores) on a glass microscope slide followed by drying in air) were performed on conjugate arrays formed on glass slides with unpolarized light at normal incident. Similarly, FT-IR spectra were collected using a Nicolet MAGNA-IR 860 spectrometer. The adsorbate-functionalized AuNPs were deposited on a polished silicon wafer and scanned 16 times at a spectral resolution of 1 cm^{-1}.

A PHI 5700 X-ray photoelectron spectrometer equipped with a monochromatic Al Kα X-ray source (hν=1486.7 eV) incident at 90° relative to the axis of a hemispherical energy analyzer was used to collect the XPS spectra of the adsorbate-functionalized AuNPs. Verification of the effectiveness of the development of the initiator-containing monolayers was conducted using HSPEG750-modified AuNPs prepared from three different sizes of nanoparticles (~15, 40, and 90 nm in diameter). For these nanoparticles, 10 mL of the aqueous suspension of AuNPs was mixed with a ~1-mM solution of HSPEG750 in EtOH (3 mL) for 30 min, and this mixture was allowed to stand at room temperature for 24 h. After washing to remove unbound adsorbate, the functionalized HSPEG750 AuNPs were then deposited onto a silicon wafer, and the solvent was allowed to evaporate before analysis. The spectrometer was operated at high resolution with a pass energy of 23.5 eV, a photoelectron takeoff angle of 45° from the surface, and an analyzer spot diameter of 2 mm. The base pressure in the chamber during the measurements was ~3×10^{-9} Torr, and the spectra were collected at room temperature. Two, eight, and 40 scans were accumulated to obtain the Au_{4f}, C_{1s}, and S_{2p} spectra, respectively. After collecting the data, the binding energies of the S_{2p} and C_{1s} peaks were determined by setting the $Au_{4f7/2}$ peak to 83.8 eV as a reference peak.

Analyses by SEM were performed using a LEO Scanning Electron Microscope with 20 kV of accelerating voltage during the measurements. To collect the images, bare AuNPs and adsorbate-functionalized AuNPs were deposited on silicon wafers and dried at room temperature. SEM was used to examine the overall morphology of both the bare and modified AuNPs. Similarly, TEM images of the nanoparticles were collected using a JEM-2000 FX electron microscope (JEOL) operating at an electron voltage of 200 kV. The samples were prepared by placing small drops of the solution onto 300-mesh holey carbon-coated copper grids and allowing the samples to dry before analysis.

Analyses by DLS were conducted on dilute samples using an ALV-5000 Multiple Tau Digital Correlation instrument operating at a light source wavelength of 514.4 nm and a fixed scattering angle of 90°. The diameters of the AuNPs and the adsorbate-functionalized AuNPs were determined from data collected at room temperature. All of the data collected showed good Gaussian distribution curves.

Results and discussion

Stability evolution of the adsorbate-functionalized AuNPs

UV–vis spectroscopy was used to investigate the stability of the adsorbate-functionalized AuNPs. According to Mie theory, AuNPs with a radius much smaller than the incident wavelength of the light will absorb at certain wavelengths

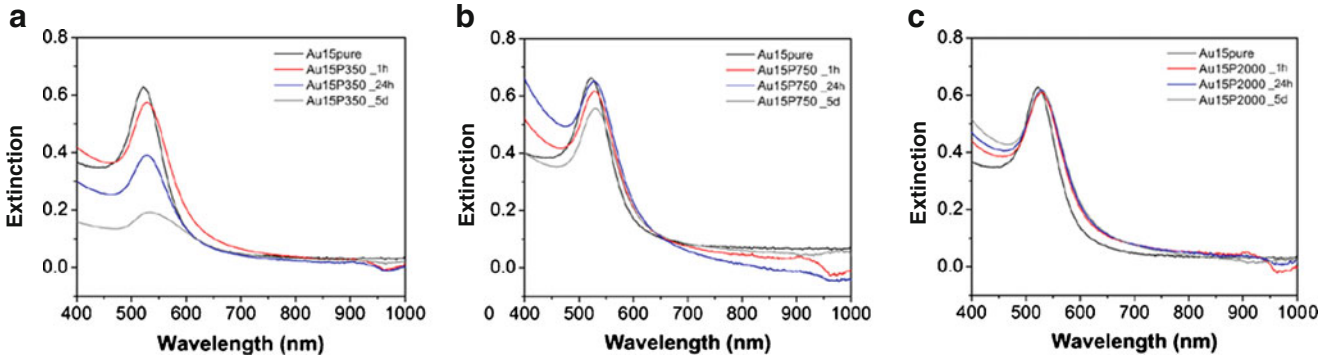

Fig. 2 UV–vis extinction spectra of bare and adsorbate-functionalized AuNPs with ~15 nm gold cores as a function of increasing time in solution where the adsorbate is **a** HSPEG350, **b** HSPEG750, and **c** HSPEG2000

due to the resonance excitation of the surface plasmons [31]. These absorption bands are strongly influenced by the particle shape, size, and the surrounding medium, along with the degree to which the particles are aggregated [24, 32]. In general, the surface plasmon resonance (SPR) band of Au spheres (about 10–50 nm in diameter) appears at around 530 nm. Increasing the diameter of these small AuNPs produces a red shift of up to ~40 nm in wavelength [15, 23]. The formation of a dielectric layer around the AuNPs will also result in a red shift of the SPR band, if the dielectric constant of the layer is larger than that of the medium [24, 33]. In addition, when the AuNPs aggregate and the distance between aggregating particles become small as compared to the particle radius, the SPR band will appear at longer wavelengths than those of the individual particles [34]. This red shifting is generally accompanied by peak broadening and a decrease in the intensity of the SPR bands. Therefore, the character of the SPR peaks provides clues regarding changes in the surface state and aggregation of AuNPs.

We monitored the SPR band in the extinction spectra as a function of time to evaluate the formation and stability of the adsorbate-functionalized AuNPs. To investigate the effect of the length of the PEG groups, three series of experimental AuNPs were studied. For each series, the size of the gold cores was kept constant, while the PEG chain lengths of the initiator molecules were varied. This approach provides comparison of the relative influence of the nanoparticle core size in contrast with that of the overlying adsorbate coating. For the extinction studies, 1 mL of each nanoparticle solution (15 nm; ~3×10^{11} particles/mL, 40 nm; ~8×10^{10} particles/mL, 90 nm; ~7×10^{9} particles/mL) was diluted twice with distilled H_2O in glass vials. Subsequently, 0.3 mL of the adsorbate solution (HS–NN–, 1 mM) in EtOH was added to the AuNP solutions (~15, 40, and 90 nm gold cores in diameter), respectively, and the mixtures were immediately agitated before recording the optical spectra to ensure the homogeneity of the solution. This process was performed for each of the different lengths of initiator-containing adsorbates (HSPEG350, HSPEG750, and HSPEG2000). Extinction spectra of each of the prepared gold sols and functionalized AuNPs were collected as a function of time. We note here that AuNPs coated with HS–NN– (but not modified with PEG) aggregated immediately, contrasting with the behavior of those modified with HSPEG350, HSPEG750, and HSPEG2000 (HSPEG350-AuNPs, HSPEG750-AuNPs, and HSPEG2000-AuNPs, respectively). Therefore, we performed no furthers studies of the stability of the HS–NN–modified AuNPs.

Figure 2a–c shows the optical spectra of the 15 nm gold core nanoparticles modified with different lengths of adsorbates. The spectrum for the as-prepared 15-nm gold sol is also

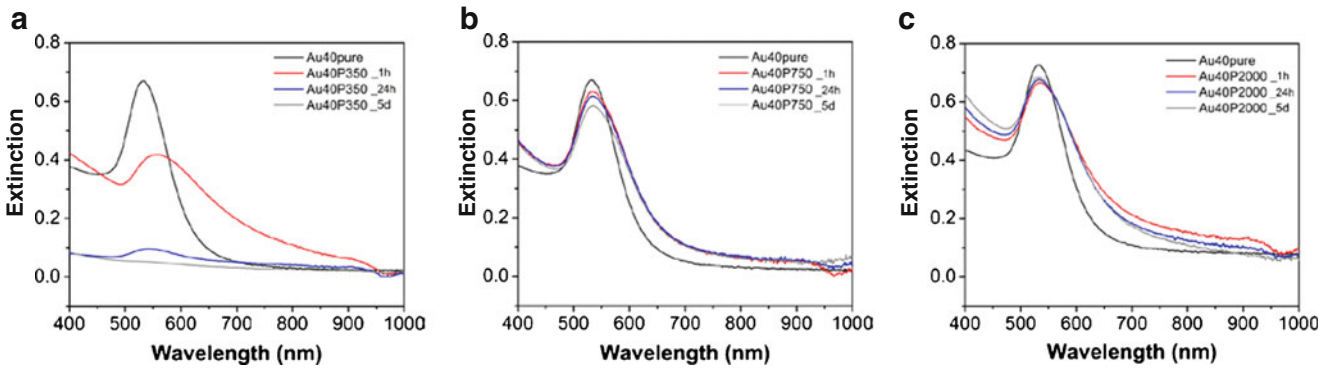

Fig. 3 UV–vis extinction spectra of bare and adsorbate-functionalized AuNPs with ~40 nm gold cores as a function of increasing time in solution where the adsorbate is **a** HSPEG350, **b** HSPEG750, and **c** HSPEG2000

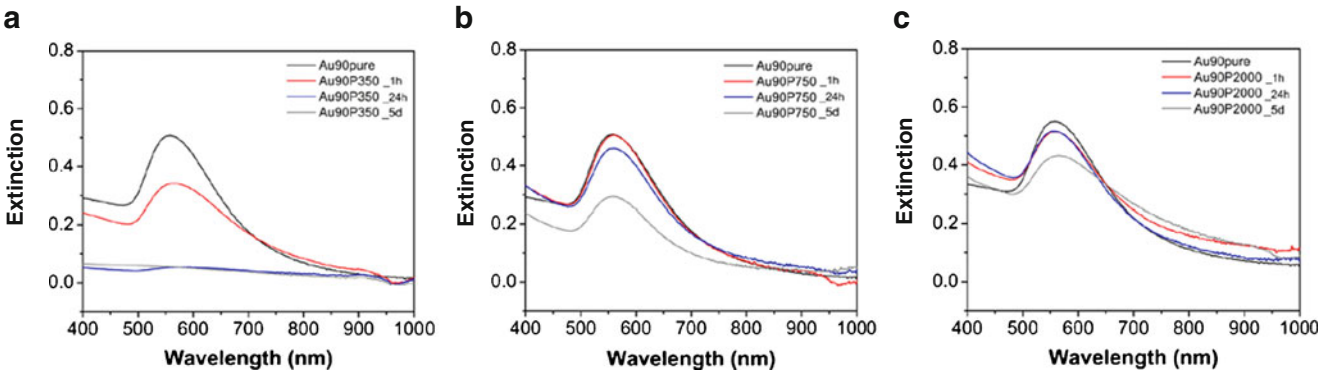

Fig. 4 UV–vis extinction spectra of bare and adsorbate-functionalized AuNPs with ~90 nm gold cores as a function of increasing time in solution, where the adsorbate is **a** HSPEG350, **b** HSPEG750, and **c** HSPEG2000

shown for comparison. In each case, the SPR band indicates a gradual red shift from 524 nm for measurements made after the adsorbates were added to the AuNP solutions, regardless of the chain length of the adsorbate, indicating the immobilization of the molecules on the surface of the AuNPs. These observations are consistent with the formation of adsorbed organic layers around the metal nanoparticles in solution [35]. For the 15-nm gold core AuNPs coated with the shortest PEG chain, HSPEG350-AuNPs, the nanoparticles started aggregating in 24 h and all of them precipitated out of suspension within 5 days. This aggregation gives rise to the dramatic decrease in the extinction maxima in the SPR bands, as shown in Fig. 2a. The rate of the aggregation is much slower for the 15-nm gold core nanoparticles functionalized with longer PEG chain adsorbates when compared to the HSPEG350-AuNPs. Interestingly, the 15-nm gold core nanoparticles with the longest PEG chains, HSPEG2000-AuNPs, showed almost no peak broadening or decrease in the intensity of the SPR band, implying that these nanoparticles undergo little or no aggregation for up to 5 days.

Differences attributable to chain length effects associated with the PEG groups were more clearly observed with the larger sizes of nanoparticles, as shown in Figs. 3 and 4. Figure 3a–c shows the optical spectra of the 40-nm gold core nanoparticles modified with different adsorbate chain lengths. The spectrum for the as-prepared gold sol is shown for comparison as well. Initially, the SPR bands of the nanoparticles red-shifted from 524 nm after the adsorbates were added to the 40-nm gold core nanoparticle solutions regardless of the chain lengths of the adsorbates, as also occurred with the HSPEG350-AuNPs. The rate of change for the SPR band appears to be inversely dependent on the PEG chain length (similar to the results obtained for the 15-nm gold core nanoparticle system), exhibiting the largest change with the shortest PEG chain. As shown in Fig. 3a, a dramatic broadening and red shifting of the SPR band to 585 nm was observed for the 40 nm gold core HSPEG350-AuNPs. It took only 1 h for the SPR band to shift to 585 nm, and substantial aggregation occurred as characterized by the broadening and decreased intensity of the SPR band. In contrast, the SPR bands of the 40-nm gold core HSPEG750-AuNPs and HSPEG2000-AuNPs show little or no SPR band broadening or diminishment, suggesting that the AuNPs modified with the longer PEG chain adsorbates undergo almost no aggregation after adsorption of these adsorbates. The 90-nm gold core nanoparticles produced a similar red-shifting trend as shown in Fig. 4a–c, and the AuNPs modified with HSPEG350 aggregated and precipitated out of suspension within 24 h. However, unlike the other two series, the 90-nm gold core nanoparticles modified with the longer adsorbates showed signs of diminished stability within 5 days.

In these studies, there was a noticeable difference in the character of the SPR bands for the initiator-modified AuNPs prepared from different lengths of PEG chains. Generally, the SPR bands in the UV–vis spectra of the HSPEG350-AuNPs were significantly broadened and red-shifted and exhibited a decrease in intensity. The HSPEG750-AuNPs and HSPEG2000-AuNPs on the 15 and 40 nm gold cores exhibited little, if any, change in the UV–vis spectra as a function of time. These observations support the notion that steric stabilization by the PEG moieties surrounding the AuNPs can play a key role in their resistance to aggregation. The PEG750 adsorbate was long enough to stabilize these two sizes of AuNPs in water for several days. Indeed, the radius of the HSPEG750-AuNPs increased the hydrodynamic radius by 5 nm for the particles in solution, as verified by DLS measurements, and this value is consistent with results reported previously [36]. However, there are indications in the data for the nanoparticles with 90 nm gold cores that the ability of the

Table 1 Summary of the colloidal stability evolution of the adsorbate-functionalized AuNPs

	HS–N=N–	HSPEG350	HSPEG750	HSPEG2000
AuNP15nm	unstable	stable	stable	stable
AuNP40nm	unstable	unstable	stable	stable
AuNP90nm	unstable	unstable	stable	stable

PEG moieties to prevent the coated AuNPs from aggregation depends on the sterically repulsive layer being of sufficient thickness to offset the underlying attractive van der Waals forces between the metal cores. The overall results regarding the stability evolution of the functionalized AuNPs are summarized in Table 1. Additional data were gathered for the HSPEG750-AuNPs, as outlined below.

Immobilization of HSPEG750 on the surface of the AuNPs

FT-IR analysis of the HSPEG750-modified AuNPs The series of HSPEG750-AuNPs were used to confirm the presence of the immobilized HSPEG750 on the surface of the gold nanoparticles by FT-IR spectroscopy, as shown in Fig. 5a. The FT-IR spectrum of pure HSPEG750 is provided for comparison. The IR spectra of the HSPEG750-AuNPs (regardless of the particle size) are similar to that of pure HSPEG750, providing evidence that HSPEG750 is indeed a part of these composite nanoparticles. The main IR bands have been identified and characterized. The prominent peak for the –C–O–C– bending bands associated with the PEG moieties was observed at 1110 cm^{-1} and the C=O bands of the ester and thioester groups were found at ~1700 cm^{-1} [37, 38]. The bands observed at 2930 and 2864 cm^{-1} correspond to the antisymmetric and symmetric stretching vibrations of the $–CH_2$ units in the PEG chain, respectively [39]. Although the IR spectra indicate that the HSPEG750 molecules were successfully grafted onto the AuNPs (noting the purification procedures for these nanoparticles that would remove any unbound thiol), it is difficult to determine the precise nature of the bonding between the AuNPs and HSPEG750 with the FT-IR spectra. To determine explicitly whether the HSPEG750 molecules are physically adsorbed or chemically bound to the AuNP surface, we collected X-ray photoelectron spectroscopy (XPS) spectra.

XPS analysis of the HSPEG750-modified AuNPs Citrate bound to gold nanoparticles, as well as planar surfaces, can be effectively displaced with a thiol-terminated monomer or polymer, by simple contact of the gold surface with a solution of these organic molecules because the covalent bond that forms between Au and S is stronger than the interaction of Au and citrate [21]. The nature of the Au–S bond in the composite particles can be evaluated by examining the binding energies of sulfur by XPS since the new bond (Au–S) influences the distribution of electrons in the atoms of interest. In particular, the S_{2p} region of the XPS spectra can provide strong evidence for bond formation between sulfur and the gold substrate. This is because the binding energy of the $S_{2p3/2}$ peak for sulfur bound to gold is known to be ~162 eV. In contrast, the $S_{2p3/2}$ peak for unbound sulfur appears at around 164 eV in the XPS spectra [40, 41], which is also associated with the $S_{2p3/2}$ peak of thioester [42]. Based on these precedents, we used XPS to confirm the immobilization of the HSPEG750 on the surface of all three AuNP gold core sizes.

XPS spectra for HSPEG750-AuNPs with gold core sizes of ~15, 40, and 90 nm were collected, and the binding energy (BE) scales for the organic layers on the AuNPs were referenced by setting the $Au_{4f7/2}$ BE to 83.8 eV. To illustrate the spectra found for these nanoparticles, the XPS spectrum of the $S_{2p3/2}$ region for the HSPEG750-AuNPs with a 40-nm gold core is shown in Fig. 5b. The presence of the covalent bond between the HSPEG750 and the AuNPs was verified with the $S_{2p3/2}$ peak at ~162 eV. The strong $S_{2p3/2}$ signal at ~164 eV can be rationalized either as an incomplete adsorbate binding of the HSPEG750 or confirmation of the presence of the thioester sulfur within the adsorbate chain. We believe the latter case given the relative attenuation of photoelectrons and their different positions around the modified AuNPs; bound thiol sulfur is at the HSPEG750-AuNP interface, and the thioester sulfur is closer to the outer surface. Attenuation in a layered structure tends to underestimate the elements buried deeper relative to those at the outer surface, resulting in a much smaller XPS intensity for the buried atoms. This would explain the smaller intensity of the $S_{2p3/2}$ peak at 162 eV associated with the bound thiol sulfur. Considering the presence of the $S_{2p3/2}$ peak at 164 eV, we cannot rule out the possibility of the presence of some unbound HSPEG750

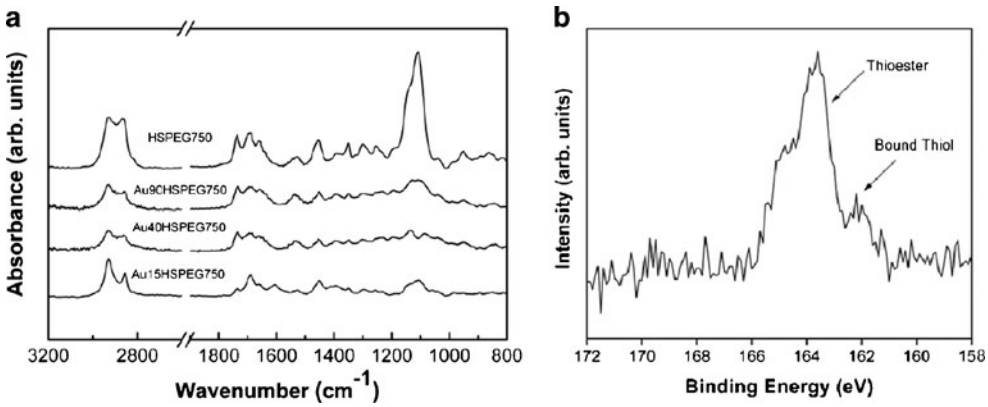

Fig. 5 **a** FT-IR spectra of the molecule HSPEG750 and the series of HSPEG750-AuNPs. **b** XPS spectra of the S_{2p} region of the HSPEG750-AuNPs with 40 nm gold cores

(unbound thiols); however, we believe that the $S_{2p3/2}$ peak at 164 eV is mainly from the thioester sulfur and that almost all of the HSPEG750s are adsorbed on the surface of the AuNPs. In order to rationalize this explanation, HSPEG750s were also immobilized on a flat gold substrate and the $S_{2p3/2}$ signal in the XPS spectrum exhibited a similar trend as that for the HSPEG750-AuNPs (data not shown).

Reversible aggregation/deaggregation of HSPEG750-functionalized AuNPs

As described in the preceding section, we showed that HSPEG750 is able to stabilize the various sizes of the AuNPs in water. Both the aqueous solubility and the general stability of these nanoparticles can be attributed to the exposed PEG moieties. However, to determine if these terminal groups contribute to aggregation under various solution conditions, we tested them further in a variety of environments. We found that the HSPEG750-AuNPs were colloidally stable not only in Milli-Q water but also in solvent-free "dried" form and could be readily redispersed in aqueous buffer solutions (pH 4, 7, and 10) and in nonaqueous solvents (EtOH, MeOH, THF, and CH_2Cl_2) without any noticeable loss to aggregation. For the preparation of the samples in Fig. 6b, one drop of each of the HSPEG750-AuNPs (~15, 40, and 90 nm gold cores) were deposited on the glass slides and dried in air. Figure 6 provides evidence of this phenomenon, showing HSPEG750-AuNPs with ~15, 40, and 90 nm gold cores (a) dispersed in aqueous solution and (b) isolated in a solvent-free "dried" form. When dispersed in aqueous solution, the HSPEG750-AuNPs exist as discrete species, producing the characteristic color associated with individual AuNPs; ruby red, purple, and brown for the ~15, 40, and 90 nm gold cores, respectively. As the solvents were evaporated, the nanoparticles began to aggregate, revealing the bulk metal color of the gold core, as shown in Fig. 6b. Moreover, the isolating–redispersing process of these nanoparticles (aggregation/deaggregation) was completely reversible; the HSPEG750-AuNPs failed to undergo fusion of the metallic cores even in the solvent-free form. Irreversible aggregation is a notorious problem for large AuNPs (>10 nm) during preparation and purification [22, 23]. Importantly, the dried monolayer-coated AuNPs described here could be redispersed in a variety of solvents without any signs of particle degradation or formation of permanent aggregates.

Along with the color changes observed by the naked eye, the optical properties of the reversibly aggregated/deaggregated HSPEG750-AuNPs were thoroughly investigated using UV–vis spectroscopy. The extinction spectra of the HSPEG750-AuNPs dispersed in aqueous solution and the nanoparticles in the solvent-free form are shown in Fig. 6c, d, respectively. As

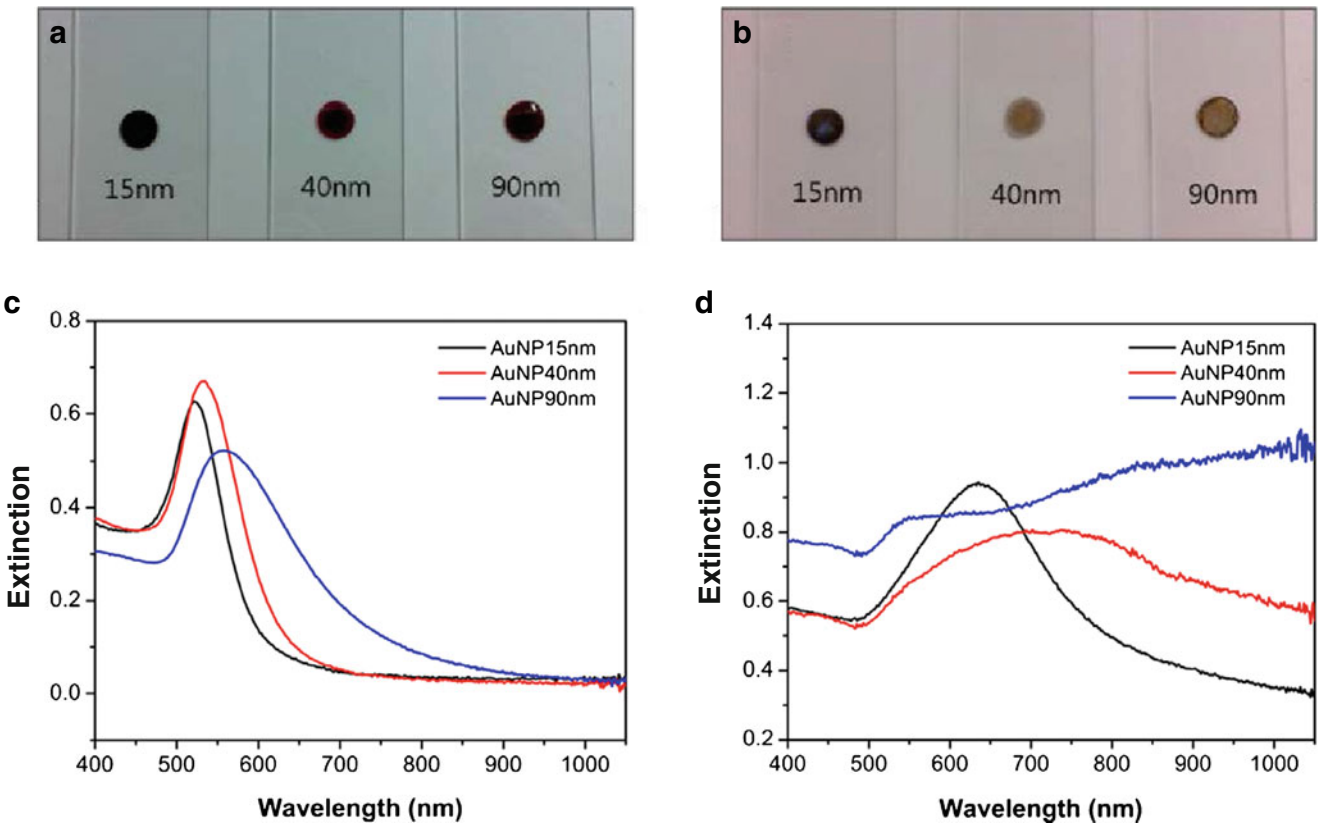

Fig. 6 Photographs of the HSPEG750-AuNPs with ~15, 40, and 90 nm diameter gold cores (from left to right): **a** in aqueous solution and **b** in solvent-free "dried" form. Extinction spectra of the HSPEG750-AuNPs in **c** aqueous solution and **d** in solvent-free "dried" form

described in the "Experimental section", the measurements for the solvent-free forms were performed on the HSPEG750-AuNPs deposited on glass slides with unpolarized light at normal incident. All of the samples in aqueous solution exhibit similar features in their extinction spectra with values of λ_{max} at 520, 530, and 600 nm (corresponding to the ~15, 40, and 90 nm diameter gold cores), which are the characteristic values for spherical AuNPs in aqueous solution [15]. In accordance with the visual observations, the HSPEG750-AuNPs in the solvent-free form show dramatically red-shifted SPR bands with values of λ_{max} at 650 and 750 nm, corresponding to the ~15 and 40 nm gold cores, and accompanied with noticeable broadening of the spectra. Additionally, the SPR band for the 90-nm gold core HSPEG750-AuNPs resulted in a broad absorption that stretches from the UV to the IR region, which is a characteristic response expected for a continuous metal film [15, 43]. These results might be attributed to a form of aggregation where the functionalized AuNPs group in aggregate characteristics of their size or to plasmon hybridization between the neighboring nanoparticles. Since simple aggregations of AuNPs in solution showed no similar dramatic red shift ($\Delta\lambda$=~120 nm) in their extinction spectra, we believe that this phenomenon is more likely related to the latter case for our system. The SEM and TEM images support this hypothesis (vide infra).

Figure 7a shows a TEM image of the ~15-nm gold core HSPEG750-AuNPs, and Fig. 7b, c shows SEM images of the ~40- and ~90-nm gold core HSPEG750-AuNPs, respectively. For the HSPEG750-AuNPs in the solvent-free form, the nanoparticles are in close proximity at a distance determined by the monolayer boundaries between the gold cores. The uniformity of the distances established by the HSPEG750 adsorbates gives an average interparticle spacing of about 3 nm as estimated from the SEM and TEM images. The resulting plasmon hybridization between neighboring individual nanoparticles in particle aggregate assemblies, produces surface plasmon bands that are more dramatically red-shifted [44]. These intermixed, hybridized plasmon bands disperse strongly to lower energies, corresponding to infrared wavelengths of the spectrum for the larger gold cores, leading to a red shift of the surface plasmon band of all three samples. These observations are in agreement with a prior report, where ordered arrays of metallic nanospheres with less than 10 nm interparticle spacing were shown to induce strong plasmon coupling of the arrayed nanoparticles [44]. As with the reversible aggregation/deaggregation observed by the naked eye, we found these optical properties to be completely reversible for our system. This unique reversibility might prove useful for chemical vapor sensing as well as for the self-assembly of monolayer-coated AuNPs in nanoscale electronic devices [45–47]. Further modification of the initiator molecule with biomolecules such as antibodies, enzymes, and DNA should provide additional applications for these nanoparticles as biosensors, affording greater flexibility in the selection of both the targeting and receptor molecules.

Conclusions

In this study, we demonstrated a successful strategy for stabilizing AuNPs with thiol-based PEG-terminated free radical initiators designed to serve as precursors in the synthesis of polymer-coated nanoparticles and as templates for the development of stable nanoparticle systems. One end of the custom-designed adsorbates was modified with PEG moieties having various chain lengths that imparted stability to nanoparticle conjugates through steric hindrance. The stability of the composite particles was evaluated both as a function of PEG chain length (Mn 350, 750, and 2,000) and AuNP gold core size (~15, 40, and 90 nm). Overall, the adsorbates with the longest PEG chains (i.e., PEG750 and PEG2000) stabilized the smaller AuNPs (~15 and 40 nm gold cores) for up to several days without marked aggregation or precipitation. In contrast, these adsorbates afforded only partial stability to the 90 nm AuNPs over the duration of our analysis. Importantly, the adsorbate-functionalized AuNPs could be isolated in solvent-free "dried" form and redispersed in various solvents, including buffered aqueous solutions (pH 4, 7, and 10), EtOH, MeOH, THF, and CH_2Cl_2. The isolating–redispersing process was found to be completely reversible, providing additional evidence of the stabilizing effect of the PEG-modified initiator molecules. The successful adsorption of the adsorbates and

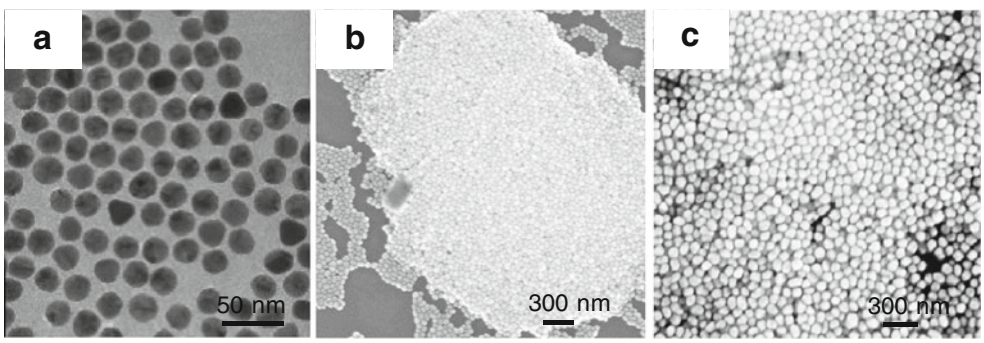

Fig. 7 **a** TEM image of the HSPEG750-AuNPs with ~15 nm gold cores in solvent-free "dried" form and SEM images of the HSPEG750-AuNPs with **b** ~40 nm and **c** ~90 nm gold cores in solvent-free form

the bonding of these molecules on the surfaces were further characterized by FT-IR and XPS spectroscopy, respectively. Notably, the method reported here can be generally applied to other nanoparticle systems (e.g., silica core/gold shell or magnetic core/gold shell nanoparticles), providing enhanced versatility in the nature of both the nanoparticle cores and the polymer shells.

Acknowledgments We gratefully acknowledge financial support from the Robert A. Welch Foundation (grant no. E-1320), the Alliance for NanoHealth (W81XWH-10-2-0125), and the Texas Center for Superconductivity at the University of Houston.

References

1. Teranishi T, Miyake M (1998) Size control of palladium nanoparticles and their crystal structures. Chem Mater 10(2):594–600
2. Quaroni L, Chumanov G (1999) Preparation of polymer-coated functionalized silver nanoparticles. J Am Chem Soc 121(45): 10642–10643
3. Chen S, Sommers JM (2001) Alkanethiolate-protected copper nanoparticles: spectroscopy, electrochemistry, and solid-state morphological evolution. J Phys Chem B 105(37):8816–8820
4. Klein DL, Roth R, Lim AKL, Alivisatos AP, McEuen PL (1997) A single-electron transistor made from a cadmium selenide nanocrystal. Nature 389(6652):699–701
5. Bergbreiter DE, Case BL, Liu YS, Caraway JW (1998) Poly(*N*-isopropylacrylamide) soluble polymer supports in catalysis and synthesis. Macromolecules 31(18):6053–6062
6. Jeong B, Bae YH, Lee DS, Kim SW (1997) Biodegradable block copolymers as injectable drug-delivery systems. Nature 388(6645): 860–862
7. Raula J, Shan J, Nuopponen M, Niskanen A, Jiang H, Kauppinen EI, Tenhu H (2003) Synthesis of gold nanoparticles grafted with a thermoresponsive polymer by surface-induced reversible-addition-fragmentation chain-transfer polymerization. Langmuir 19(8):3499–3504
8. Ohno K, Koh K, Tsujii Y, Fukuda T (2002) Synthesis of gold nanoparticles coated with well-defined, high-density polymer brushes by surface-initiated living radical polymerization. Macromolecules 35(24):8989–8993
9. Mandal TK, Fleming MS, Walt DR (2002) Preparation of polymer coated gold nanoparticles by surface-confined living radical polymerization at ambient temperature. Nano Lett 2(1):3–7
10. Nuβ S, Böttcher H, Wurm H, Hallensleben ML (2001) Gold nanoparticles with covalently attached polymer chains. Angew Chem Int Ed 40(21):4016–4018
11. Connor EE, Mwamuka J, Gole A, Murphy CJ, Wyatt MD (2005) Gold nanoparticles are taken up by human cells but do not cause acute cytotoxicity. Small 1(3):325–327
12. DE Owens III, Peppas NA (2006) Opsonization, biodistribution, and pharmacokinetics of polymeric nanoparticles. Int J Pharm 307(1):93–102
13. Phillips MA, Gran ML, Peppas NA (2010) Targeted nanodelivery of drugs and diagnostics. Nano Today 5(2):143–159
14. Daniel M-C, Astruc D (2004) Gold nanoparticles: assembly, supramolecular chemistry, quantum-size-related properties, and applications toward biology, catalysis, and nanotechnology. Chem Rev 104(1):293–346
15. Liz-Marzán LM (2006) Tailoring surface plasmons through the morphology and assembly of metal nanoparticles. Langmuir 22(1):32–41
16. Mossmer S, Spatz JP, Möller M, Aberle T, Schmidt J, Burchard W (2000) Solution behavior of poly(styrene)-block-poly(2-vinylpyridine micelles containing gold nanoparticles. Macromolecules 33(13): 4791–4798
17. Miyazaki A, Nakano Y (2000) Morphology of platinum nanoparticles protected by poly(*N*-isopropylacrylamide). Langmuir 16(18):7109–7111
18. Birdi KS (1998) Handbook of surface and colloid chemistry. CRC Press, Boca raton
19. Green SJ, Stokes JJ, Hostetler MJ, Pietron J, Murray RW (1997) Three-dimensional monolayers: nanometer-sized electrodes of alkanethiolate-stabilized gold cluster molecules. J Phys Chem B 101(14):2663–2668
20. Mirkin CA (2000) Programming the assembly of two- and three-dimensional architectures with DNA and nanoscale inorganic building blocks. Inorg Chem 39(11):2258–2272
21. Oldenburg SJ, Averitt RD, Westcott SL, Halas NJ (1998) Nanoengineering of optical resonances. Chem Phys Lett 288(2–4): 243–247
22. Weisbecker CS, Merritt MV, Whitesides GM (1996) Molecular self-assembly of aliphatic thiols on gold colloids. Langmuir 12(16):3763–3772
23. Resch R, Baur C, Bugacov A, Koel BE, Echternach PM, Madhukar A, Montoya N, Requicha AAG, Will P (1999) Linking and manipulation of gold multinanoparticle structures using dithiols and scanning force microscopy. J Phys Chem B 103(18):3647–3650
24. Aslan K, Perez-Luna VH (2002) Surface modification of colloidal gold by chemisorption of alkanethiols in the presence of a nonionic surfactant. Langmuir 18(16):6059–6065
25. Sistach S, Rahme K, Perignon N, Marty JD, Viguerie NLD, Gauffre F, Mingotaud C (2008) Bolaamphiphile surfactants as nanoparticle stabilizers: application to reversible aggregation of gold nanoparticles. Chem Mater 20(4):1221–1223
26. Wuelfing WP, Gross SM, Miles DT, Murray RW (1998) Nanometer gold clusters protected by surface-bound monolayers of thiolated poly(ethylene glycol) polymer electrolyte. J Am Chem Soc 120(48):12696–12697
27. Schneider G, Decher G (2008) Functional core/shell nanoparticles via layer-by-layer assembly. Investigation of the experimental parameters for controlling particle aggregation and for enhancing dispersion stability. Langmuir 24(5):1778–1789
28. Lin S-Y, Tsai Y-T, Chen C-C, Lin C-M, Chen C-H (2004) Two-step functionalization of neutral and positively charged thiols onto citrate-stabilized au nanoparticles. J Phys Chem B 108(7):2134–2139
29. Park HH, Lee TR (2011) Thermo- and pH-responsive hydrogel-coated gold nanoparticles prepared from rationally designed surface-confined initiators. J Nanopart Res 13(7):2909–2918
30. Frens G (1973) Controlled nucleation for regulation of particle-size in monodisperse gold suspensions. Nat Phys Sci 241(105):20–22
31. Kreibig U, Vollmer M (1995) Optical properties of metal cluster. Springer, New York
32. Mulvaney P (1996) Surface plasmon spectroscopy of nanosized metal particles. Langmuir 12(3):788–800
33. Stuart DA, Haes AJ, Yonzon CR, Hicks EM, Van Duyne RP (2005) Biological applications of localised surface plasmonic phenomenae. IEE Proc. Nanobiotechnol 152(1):13-32
34. Rahme K, Gauffre F, Marty JD, Payre B, Mingotaud C (2007) A systematic study of the stabilization in water of gold nanoparticles by poly(ethylene oxide)-poly(propylene oxide)-poly(ethylene oxide) triblock copolymers. J Phys Chem C 111(20):7273–7279
35. Eck D, Helm CA, Wagner NJ, Vaynberg KA (2001) Plasmon resonance measurements of the adsorption and adsorption kinetics of a biopolymer onto gold nanocolloids. Langmuir 17(4):957–960

36. Liu YL, Shipton MK, Ryan J, Kaufman ED, Franzen S, Feldheim DL (2007) Synthesis, stability, and cellular internalization of gold nanoparticles containing mixed peptide-poly(ethylene glycol) monolayers. Anal Chem 79(6):2221–2229
37. Cao C, Sim SJ (2007) Preparation of highly stable oligo(ethylene glycol) derivatives-functionalized gold nanoparticles and their application in lspr-based detection of psa/act complex. J Nanosci Nanotechnol 7(11):3754–3757
38. Li DX, He Q, Zhu HF, Tao C, Li JB (2007) Enhanced dispersity of gold nanoparticles modified by omega-carboxyl alkanethiols under the impact of poly(ethylene glycol)s. J Nanosci Nanotechnol 7(9):3089–3094
39. Manna A, Imae T, Yogo T, Aoi K, Okazaki M (2002) Synthesis of gold nanoparticles in a winsor ii type microemulsion and their characterization. J Colloid Interface Sci 256(2):297–303
40. Castner DG, Hinds K, Grainger DW (1996) X-ray photoelectron spectroscopy sulfur 2p study of organic thiol and disulfide binding interactions with gold surfaces. Langmuir 12(21):5083–5086
41. Laibinis PE, Whitesides GM, Allara DL, Tao YT, Parikh AN, Nuzzo RG (1991) Comparison of the structures and wetting properties of self-assembled monolayers of normal-alkanethiols on the coinage metal-surfaces, cu, ag, au. J Am Chem Soc 113(19):7152–7167
42. Wenzler LA, Moyes GL, Raikar GN, Hansen RL, Harris JM, Beebe TP, Wood LL, Saavedra SS (1997) Measurements of single-molecule bond rupture forces between self-assembled monolayers of organosilanes with the atomic force microscope. Langmuir 13(14): 3761–3768
43. Ung T, Liz-Marzán LM, Mulvaney P (2001) Optical properties of thin films of au@sio2 particles. J Phys Chem B 105(17):3441–3452
44. Wang H, Kundu J, Halas NJ (2007) Plasmonic nanoshell arrays combine surface-enhanced vibrational spectroscopies on a single substrate. Angew Chem Int Ed 46(47):9040–9044
45. Jin CM, Zhou HH, Wei W, Narayan R (2006) Three-dimensional self-organization of crystalline gold nanoparticles in amorphous alumina. Appl Phys Lett 89(26):261103/1–261103/3
46. Hutchinson TO, Liu Y-P, Kiely C, Kiely CJ, Brust M (2001) Templated gold nanowire self-assembly on carbon substrates. Adv Mater 13(23):1800–1803
47. Hassenkam T, Norgaard K, Iversen L, Kiely CJ, Brust M, Bjornholm T (2002) Fabrication of 2d gold nanowires by self-assembly of gold nanoparticles on water surfaces in the presence of surfactants. Adv Mater 14(16):1126–1130